ChemPubSoc Europe

DOI: 10.1002/open.201900139

Open Access ChemistryOPEN Full Papers

SAMBADENA Hyperpolarization of ^{13}C-Succinate in an MRI: Singlet-Triplet Mixing Causes Polarization Loss

Stephan Berner,*[a, b, c] Andreas B. Schmidt,[a, d] Mirko Zimmermann,[a] Andrey N. Pravdivtsev,[d] Stefan Glöggler,[e, f] Jürgen Hennig,[a] Dominik von Elverfeldt,[a] and Jan-Bernd Hövener*[d]

The signal enhancement provided by the hyperpolarization of nuclear spins of biological molecules is a highly promising technique for diagnostic imaging. To date, most ^{13}C-contrast agents had to be polarized in an extra, complex or cost intensive polarizer. Recently, the *in situ* hyperpolarization of a ^{13}C contrast agent to >20% was demonstrated without a polarizer but within the bore of an MRI system. This approach addresses some of the challenges of MRI with hyperpolarized tracers, i.e. elevated cost, long production times, and loss of polarization during transfer to the detection site. Here, we demonstrate the first hyperpolarization of a biomolecule in aqueous solution in the bore of an MRI at field strength of 7 T within seconds. The ^{13}C nucleus of 1-^{13}C, 2,3-$^{2}H_2$-succinate was polarized to 11% corresponding to a signal enhancement of approximately 18.000. Interesting effects during the process of the hydrogenation reaction which lead to a significant loss of polarization have been observed.

1. Introduction

Magnetic Resonance Imaging (MRI) and spectroscopy (MRS) are powerful tools in clinical routine and diagnosis. However, clinical MRI is limited to proton (^{1}H) imaging due to the low natural abundance and low thermal polarization of other nuclei. In fact, even for ^{1}H, no more than a few parts per million of all spins effectively contribute to the MR signal in a field of 1 T. The low proton polarization ($P \approx 10^{-6}$) is partially compensated by the high proton concentration in living tissues, ~80 M, mostly water and lipids. Along with sophisticated imaging methods and hardware, a sufficient signal to noise ratio (SNR) is obtained that enables anatomical, functional and dynamical proton imaging *in vivo*.[1–3]

For other (X–) nuclei, like ^{13}C, ^{15}N or ^{17}O, the situation is different: their polarization, concentration and natural abundance are (much) lower than for ^{1}H. As a result, the SNR is not sufficient for fast imaging, and spatial and temporal resolutions are poor. If imaging is feasible, long measurement times are required[4–6] (e.g. 30 minutes acquisition time for ^{17}O brain MRI at 3 T with 300 averages, 5.6 mm isotropic resolution and an SNR of 36).[7]

The hyperpolarization of nuclear spins is a promising method to boost the MR signal of any MR active nucleus by several orders of magnitude. The most prominent method, dissolution Dynamic Nuclear Polarization (d-DNP),[8] is commercially available and is extensively applied *in vivo* with great promise.[9–12] At the same time, the method is inherently expensive, relatively slow and requires an external polarizer. Another approach, *ParaH*ydrogen Induced Polarization (PHIP[13–15]), is much less costly and much faster, but less developed with respect to *in vivo* application. PHIP is based on the spin order of *para*hydrogen (pH_2), the spin singlet isomer of dihydrogen. *Bowers* and *Weitekamp* suggested transferring singlet spin order into strongly enhanced magnetization after hydrogenation (Parahydrogen and Synthesis Allow Dramatically Enhanced Nuclear Alignment, PASADENA)[15] in the 1980s. Various stand-alone PASADENA polarizers were developed to transfer the pH_2 spin order into observable polarization at low magnetic field (nT – mT range) since 2004.[16–26] Both d-DNP and PHIP require a stand-alone polarizer and transfer of the polarized substrate to the Nuclear Magnetic Resonance (NMR) spectrometer or MRI system. Hence, relaxation during transfer decreases the available level of spin polarization.

Recently, Synthesis Amid the Magnet Bore Allows Dramatically Enhanced Nuclear Alignment (SAMBADENA)[27] was presented, where the hydrogenation, polarization transfer, and

[a] S. Berner, A. B. Schmidt, M. Zimmermann, Prof. Dr. Dr. h.c. J. Hennig, PD Dr. D. von Elverfeldt
Department of Radiology, Medical Physics,
Medical Center – University of Freiburg, Faculty of Medicine, University of Freiburg
Killianstraße 5a, 79106 Freiburg, Germany
E-mail: Stephan.berner@uniklinik-freiburg.de
[b] S. Berner
German Consortium for Cancer Research (DKTK)
partner site Freiburg
[c] S. Berner
German Cancer Research Center (DKFZ)
Im Neuenheimer Feld 280, 69120 Heidelberg, Germany
[d] A. B. Schmidt, Dr. A. N. Pravdivtsev, Prof. Dr. J.-B. Hövener
Department of Radiology and Neuroradiology, Section Biomedical Imaging, MOIN CC, University Medical Center Schleswig-Holstein, University of Kiel
Am Botanischen Garten 14, 24118 Kiel, Germany
E-mail: jan.hoevener@rad.uni-kiel.de
[e] Dr. S. Glöggler
Max Planck Institute for Biophysical Chemistry
Am Fassberg 11, 37077 Göttingen, Germany
[f] Dr. S. Glöggler
Center for Biostructural Imaging of Neurodegeneration
Von-Siebold-Straße 3a, 37075 Göttingen, Germany

Supporting information for this article is available on the WWW under https://doi.org/10.1002/open.201900139

detection of the hyperpolarized signal takes place within seconds in the bore of an MRI system. So far, a xenobiotic ^{13}C-tracer, 1-^{13}C, 2,3,3-$^{2}H_3$-hydroxyethyl-propionate (HEP), was polarized by SAMBADENA to a ^{13}C polarization of ~21% within seconds, and applied for *ex vivo*[27] and *in vivo*[28] imaging. In this article, we present the SAMBADENA hyperpolarization of the biomolecule 1-^{13}C, 2,3-$^{2}H_2$-succinate (SUC) to ~11% in the magnet bore of a preclinical MRI system at a field strength of 7 T. Succinate is an intermediate in the tricarboxylic acid (TCA) cycle and may be used for the diagnosis of brain cancer.[29–31] New insights into the spin chemistry of the hydrogenation reaction and singlet-triplet mixing were gained, which have a strong impact on the singlet spin order and thus polarization.

Methods

Spin Order Transfer Sequences

Various field cycling[16,25,32] or spin order transfer (SOT) sequences[33–41] were described to transfer spin order from pH_2 into detectable magnetization of a nearby spin-$^1/_2$ target nucleus (X) after hydrogenation. These SOT sequences consist of a train of appropriate radio frequency pulses on ^{1}H and the target nucleus X interleaved by free evolution intervals (Figure 1). Polarization transfer is achieved via the scalar spin-spin interaction (J-coupling) network.

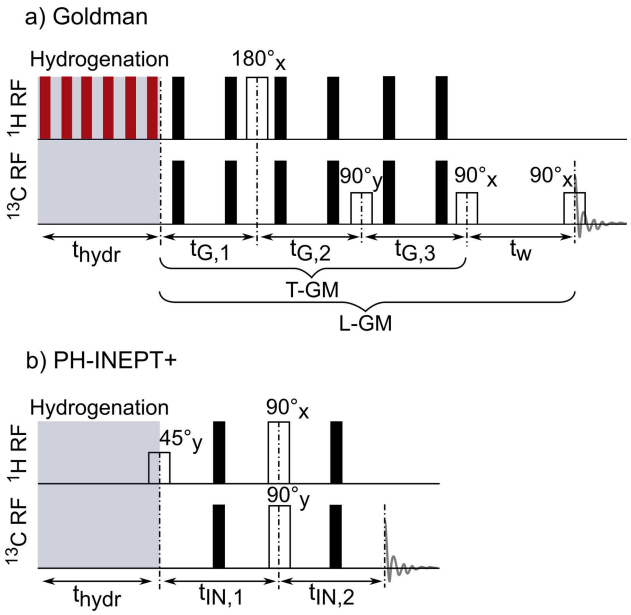

Figure 1. Pulse sequences used for the hyperpolarization of SUC after hydrogenation. Goldman's sequence (a) and PH-INEPT+ (b) are depicted as described in the original publications.[33,34] Black bars denote 180°$_x$ echo pulses. The sequence reported by Goldman *et. al.* was designed to act on the full singlet spin order (I_1·I_2), and thus heteronuclear decoupling (indicated by red bars) on the ^{1}H channel was applied during hydrogenation (here, MLEV16[42]). Contrary, PH-INEPT+ was designed for longitudinal spin order $I_{1z}I_{2z}$. Therefore, no decoupling was applied so that longitudinal spin order $I_{1z}I_{2z}$ prevailed after the hydrogenation.

SOT Sequences for Weakly Coupled Protons

The sequences PH-INEPT+[33] (Figure 1b) and Efficient Spin Order Transfer To Heteronuclei via Relayed INEPT Chains (ESOTHERIC)[40] were designed for systems with weakly coupled protons to transfer longitudinal double spin order into polarization of the target nuclei. Here, double spin order takes the form $I_{1z}I_{2z}$, where $I_{i,z}$ indicates the longitudinal spin operator of the i^{th} proton.

In the original contributions,[33,40] it was assumed that, during the hydrogenation, the transversal $I_{1x}I_{2x}$- and $I_{1y}I_{2y}$-components of the singlet order are lost because of incoherent free evolution, and that only $I_{1z}I_{2z}$ order survives.[33,40] This is largely valid for ABX-spin systems (two chemically non-equivalent hydrogens A and B and one carbon X), where the protons are weakly coupled (i.e. where the chemical shift difference, $\Delta\nu_{12}$, between the protons A and B is much larger than their mutual proton-proton J-coupling, J_{12}; $\Delta\nu_{12} \gg J_{12}$).

SOT Sequences for Strongly Coupled Protons

On the other hand, there is another class of SOT sequences designed to transfer polarization in systems with strongly coupled or chemically equivalent protons, e.g. in AA'X spin systems.[34–39,41] In these systems, the chemical shift difference between the protons A and A' is much smaller than the coupling ($\Delta\nu_{12} \ll J_{12}$) or equal to zero. Goldman's sequence[34] (Figure 1a) was designed to transfer the full singlet order I_1·I_2 of pH_2 into magnetization in AA'X spin systems (two chemically but not magnetically equivalent hydrogens and one carbon). Decoupling during the hydrogenation was suggested to reduce the loss of spin order arising from J_{AX} and $J_{A'X}$ interactions. Here, we denote the full Goldman sequence by "L-GM". L-GM generates longitudinal magnetization, which is read out after a period t_w by another pulse-acquisition experiment. The sequence without the last pulse (after the 3rd free evolution interval) is denoted by "T-GM" (see Figure 1a). In this case, transversal magnetization is generated and directly recorded.

Simulations

Hamiltonian

Quantum mechanical simulations were performed to predict optimal SOT parameters and the theoretical polarization yield using the density matrix formalism and a custom written simulation tool (MatLab 2015b, MathWorks, USA). The double deuterated SUC used here was approximated as a three spin-$^1/_2$ system (two protons and one carbon). The deuterium nuclei and couplings were neglected because the ^{1}H-^{1}H- and ^{1}H-^{13}C-coupling are much stronger than ^{2}H-^{1}H and ^{2}H-^{13}C couplings. This, of course, is a simplification. Note that the chemical shifts of the protons added during the hydrogenation (fumarate to succinate) are identical due to the symmetry of the molecule. The system was driven by the isotropic, liquid-state Hamiltonian, which reads in the laboratory frame of reference as:

$$H/h = -\nu_I(I_{1z} + I_{2z}) - \nu_S S_z + \left[J_{12}(I_1 \cdot I_2) + \sum_{k=1}^{2} J_{kS} I_{kz} S_z\right] \quad (1)$$

$$\text{with } I_1 \cdot I_2 = I_{1z}I_{2z} + I_{1y}I_{2y} + I_{1x}I_{2x} \quad (2)$$

I_1, I_2 and S are the spin operators of two protons and one carbon, respectively. The ^{1}H and ^{13}C Larmor frequencies are indicated by ν_I

and ν_S; $I_{k,z}$ and S_z denote the longitudinal spin operators of the protons and ^{13}C, respectively. I_{kx} and I_{ky} (k = 1 or 2) are transversal proton spin operators. The J-couplings of SUC were taken from literature[43,44] as $J_{12} = 7.41$ Hz, $J_{1S} = 5.82$ Hz and $J_{2S} = -7.15$ Hz for pH = 2.9. Strong proton-proton ($I_1 \cdot I_2$) and weak proton-carbon J-couplings ($I_{kz}S_z$ with k = 1 or 2) were assumed.

Density Matrix, Hydrogenation and Singlet-Triplet Mixing

The density matrix of two protons in singlet state reads[34]

$$\rho_{pH_2} = \frac{1}{4}E - I_1 \cdot I_2 \tag{3}$$

where E is the unity operator.

In a naive model, the system after hydrogenation with pH_2 is described by the direct product of the protons and the target nucleus ^{13}C in thermal equilibrium (Eq. 4):

$$\rho_S = \rho_{pH_2} \otimes \rho_{^{13}C} \tag{4}$$

The thermal polarization of ^{13}C was assumed to be zero, i.e. $\rho_{^{13}C}$ is a normalized 2×2 unity matrix with diagonal matrix elements of the value 0.5 and zero off-diagonal elements.

For a more realistic picture, the process of hydrogenation was considered: as the reaction takes place over a finite period of time, each hydrogenated molecule experiences a different evolution time. This condition is approximated by calculating a time-averaged density matrix

$$\overline{\rho_S} = \frac{\sum_{t=n\cdot\Delta t}^{t_{hydr}} p(t) Q_t \rho_S Q_t^{\dagger}}{\sum_{t=n\cdot\Delta t}^{t_{hydr}} p(t)} \tag{5}$$

where p(t) is a weighting function that reflects the amount of hydrogenated molecules at different points in time. The hydrogenation time t_{hydr} was set to 5 s and $\Delta t = 0.001$ s is the time increment of the calculations. N is an integer number from 1 to 5000. Q_t is an operator that either describes the evolution under heteronuclear decoupling (MLEV16[42]) or periods of free evolution. During the hydrogenation reaction (5 s), 100 complete MLEV16-cycles were executed. The length of a single 90° excitation pulse was $t_{MLEV,90^\circ} = 781$ µs.

Note that if Q_t is set to free evolution, the numerical results obtained are equivalent to the analytical expression derived by Natterer *et al.*[45] (Eq. 6):

$$\overline{\rho_S} = \frac{1}{4}E - I_{1z}I_{2z} - \bar{a}\left(I_{1x}I_{2x} + I_{1y}I_{2y}\right) - \bar{c}\left(I_{1z} - I_{2z}\right)S_z$$

$$\text{with } \bar{a} = \left(\frac{J_{12}}{J'}\right)^2,\ \bar{c} = \frac{J_{12}J_\Delta}{J'^2},\ J_\Delta = \frac{J_{1S} - J_{2S}}{2} \tag{6}$$

$$\text{and } J' = \sqrt{J_{12}^2 + J_\Delta^2}$$

This expression is independent of the weighting function p(t). Furthermore, singlet-triplet (S-T_0) mixing may occur due to the formation of reaction intermediates at the catalyst. Hence, the time-averaged density matrix is modified to (Eq. 7):[45]

$$\overline{\rho_{S/T_0}} = \frac{1}{4}E - I_{1z}I_{2z} - \lambda\left[\bar{a}\left(I_{1x}I_{2x} + I_{1y}I_{2y}\right) + \bar{c}\left(I_{1z} - I_{2z}\right)S_z\right] \tag{7}$$

The mixing parameter λ takes real values from -1 to $+1$ and depends on the contact time with the catalyst and chemical shift difference of the two protons in the intermediate state during hydrogenation. For $\lambda = 1$ or $\lambda = -1$, a pure time-averaged singlet or triplet state is obtained, respectively. By assuming S-T_0 mixing and heteronuclear decoupling during hydrogenation, i.e. $J_{1S} \rightarrow 0$ and $J_{2S} \rightarrow 0$, the density matrix takes the form

$$\rho_{S/T_0}^{DEC} = \frac{1}{4}E - I_{1z}I_{2z} - \lambda\left(I_{1x}I_{2x} + I_{1y}I_{2y}\right) \tag{8}$$

Hence, the quantum state after hydrogenation along with heteronuclear decoupling is determined by the parameter λ only.

Simulations of Pulse Sequences and NMR Spectra

To simulate the effect of decoupling and SOT sequences, rotation and time evolution operators were applied to the density matrix as described elsewhere.[46]

Pulses of duration t_p were approximated by an instantaneous rotation and subsequent time evolution of duration t_p. For the SOT sequence, we used ideal rotations and neglected other effects like relaxation and imperfection of RF pulses. Thus, most observed effects can be attributed to the processes during the hydrogenation. The duration of the free-evolution intervals in the SOT sequences were obtained by analytical expressions[43] and numerical optimization (MatLab 2015b, MathWorks, USA).

The theoretical polarization (in percentage) was obtained by taking the trace over the matrix product of the final density matrix after SOT and the polarization operator and subsequent multiplication by 100. The normalized polarization operators are given by $2S_z$ or $2(S_x + iS_y)$ for longitudinal or transversal polarization, respectively.

^{1}H-NMR spectra were obtained by simulating the free induction decay (FID). 2000 expectation values of the transversal magnetization ($\sum_{j=1}^{2} I_{jx} + iI_{jy}$) of the protons, interleaved by a 12.5 ms interval of free evolution, were calculated. 2000 zeros were added at the end of the data, resulting in a total data vector of 4000 complex values of 50 s. A mono-exponential decay function with a decay constant of $T_2^* = 0.1$ s was multiplied to the data to simulate transversal relaxation. The final spectrum was obtained by Fourier transformation.

Experiments

Experiments Using an MRI System

MRI System: Experiments were performed using a preclinical small animal 7 T MRI system (Biospec 7/20, PV5.1, Bruker, Germany) and a dual channel ^{1}H/^{13}C volume resonator (Rapid Biomed, Germany) with 7.2 cm inner diameter and 10 cm length of the coil. For tuning and matching of the coil, the reactor (which was used for hyperpolarization experiments) was filled with 1 mL of H_2O and placed in the isocenter of the MRI system. Subsequently, the field homogeneity was adjusted by an automatic first order shimming routine, yielding a line width of the H_2O resonance of ≈20–30 Hz. The ^{1}H and ^{13}C centre frequencies were set to 2.7 ppm and ≈176 ppm with regard to the ^{1}H resonance of H_2O at 4.7 ppm. and the ^{13}C resonance of 1-^{13}C sodium acetate at ≈182 ppm (c =

8.02 mmol in aqueous solution, CAS: 23424-28-4, Sigma Aldrich, USA).

^{1}H heteronuclear decoupling was played out during hydrogenation and data acquisition. The pulse length of a 90° excitation in the decoupling scheme is denoted by $t_{MLEV,90°}$. The amplitude and frequency (centered at 2.7 ppm) of the decoupling sequence MLEV16[42] was varied. The same parameters were used for decoupling during hydrogenation and data acquisition (676 ms acquisition time and 330 µs dwell time for ^{13}C).

pH_2 Enrichment: The pH_2 fraction of H_2 gas (99.999% purity, Sauerstoffwerk Friedrichshafen GmbH, Germany) was enriched to ~90% at 21 K using a custom made pH_2 converter.[47] The gas was stored in 0.5 L aluminium or 2.7 L steel bottles at 40 to 50 bars and used within several hours.

Sample Preparation: 1-^{13}C,2,3-$^2H_2$-succinate was formed by hydrogenation of 1-^{13}C,2,3-$^2H_2$-fumarate (FUM, MW 118.08 g·mol^{-1}, CAS: 24461–32-3, Cambridge Isotope Laboratories, MA, USA) using a rhodium based water soluble catalyst as described previously:[27] 1,4-bis-[(phenyl-3-propane sulfonate) phosphine] butane disodium salt (Q36333, MW 562.5 g·mol^{-1}, Sigma Aldrich, MO, USA) with a rhodium complex (bis(norbornadiene)rhodium (I) tetrafluoroborate, MW 373.99 g mol^{-1}, CAS: 36620-11-8, StremChemicals, MA, USA) in degassed and deionized H_2O (Figure 2). All chemicals were used without further purification.

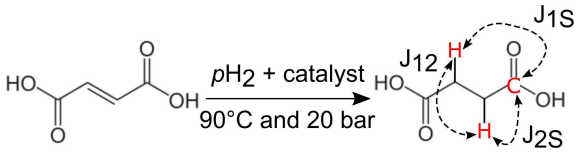

Figure 2. Schematic view of the hydrogenation reaction of FUM to SUC. pH_2 is added to FUM via a Rh-catalyst at 90 °C and 20 bar. After hydrogenation, spin order is transferred from pH_2 into ^{13}C-magnetization by means of pulse sequences and the J-coupling network. Note that the protons do not reveal a chemical shift difference.

To achieve a high hydrogenation temperature and to avoid a temperature-driven degeneration of the catalyst at the same time, two solutions were prepared: a highly concentrated catalyst "stock" solution which was kept at room temperature ($c_{rhodium}$ = 20 mM, c_{ligand} = 22 mM), and a precursor solution that was heated to ~90 °C. Only shortly before the experiment, both solution were mixed.

The precursor solution was prepared by dissolving FUM in an aqueous phosphate-buffer solution (5 mM FUM, 40 mM potassium dihydrogen phosphate KH_2PO_4, CAS: 7778-77-0; and 11 mM phosphoric acid H_3PO_4, CAS: 7664-38-2). The resulting pH value before hydrogenation was 2.9 (pH meter: HI 83141, Hanna instruments, USA)

Experimental Setup: A detailed description of the basic setup and experimental routine was published before.[27] Here two different fluidic setups 1 and 2 (Figure 3) were used for experiments on the MRI system.

For setup 1 (Figure 3a), the pH_2 bottle was connected to the inlet at the bottom of the reactor (made from Polysulfone (PSU 1000), 2 mL inner volume) via a pressure regulator, a valve (V1, type 0124, Bürkert, Germany) and PTFE (polytetrafluoroethylene) capillaries (dimensions: outer diameter 1/8'' and inner diameter 1/16'', SCP GmbH, Germany). The outlet tube (PTFE) of the reactor (1/16''× 0.75 mm, SCP GmbH, Germany) was connected to a second valve

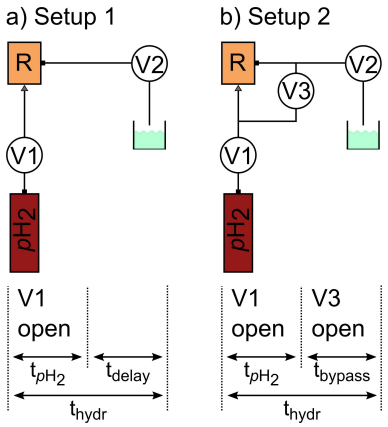

Figure 3. Setups (top) and time tables (bottom) used for SAMBADENA. Setup 1: The pH_2 reservoir was connected to the inlet of the reaction chamber (R). Valve V1 was opened for a period of t_{pH2} to initialize the chemical reaction. The SOT sequences were executed after an additional delay (t_{delay}), resulting in a total hydrogenation time t_{hydr}. After detection of the hyperpolarized signal, valve V2 was opened to clear the system. Setup 2: In addition to setup 1, a bypass was installed to equalize the pressure after t_{pH2}, reducing the bubbling. V3 was opened after t_{pH2} for time duration t_{bypass}.

(V2), used to release pressure after the experiment. For setup 2 (Figure 3b), an extra tube was added, connecting inlet and outlet via a third valve (V3). This modification was used to equilibrate the pressure between the inlet and outlet of the reactor after hydrogenation. This way, foaming was reduced, field homogeneity was improved, and less solution was flushed out of the reactor.

Experimental Workflow: Prior to each experiment, the reactor and precursor-buffer solution (900 µL) were placed in boiling water (~100 °C) for minimum two minutes. Shortly before the experiment, the precursor-buffer solution (900 µL) and concentrated catalyst solution (100 µL) were filled into the reactor. The reactor was closed and placed in the isocenter of the MRI. Next, hydrogenation was started by opening V1 for t_{pH2} = 2 s.

Using setup 1, a waiting period t_{delay} = 3 s was added after t_{pH2} before the SOT sequence was applied. Using setup 2, the bypass (V3) was opened for t_{bypass} = 3 s after t_{pH2} to equalize the pressure on in- and outlet before the SOT was applied. Thus, the total hydrogenation time was t_{hydr} = 5 s in both cases.

The valves were controlled by a custom-written software tool (MatLab 2015b, MathWorks, USA) and a data acquisition board (DAQ 6125, National Instruments, USA) connected to a power relay.

Several different combinations of setups, parameters and SOT sequences were investigated (experiments E1–E6, Table 1). Experi-

Table 1. Performed experiments on the MRI system. Experiments E1 to E6 were conducted with different SOT sequences, two different setups and decoupling parameters. For all experiments, the timings were chosen as t_{pH2} = 2 s and t_{delay} = 3 s or t_{bypass} = 3 s for setup 1 and setup 2, respectively. MLEV16 decoupling was applied during data acquisition.

	SOT	Setup	MLEV16 during hydrogenation	t_w / s
E1	PH-INEPT+	1	no	
E2	L-GM	1	no	1
E3	L-GM	1	Variation of decoupling amplitude	1
E4	T-GM	2	Variation of decoupling amplitude or frequency	
E5	L-GM	2	$t_{MLEV,90°}$ = 1 ms during t_{bypass} only	1
E6	L-GM	2	$t_{MLEV,90°}$ = 1 ms during t_{pH2} and t_{bypass}	1

ment E5 was repeated 14 times to determine the reproducibility of the polarization method. On consecutive measurement days, substrate and pH_2 was freshly prepared. The ^{13}C hyperpolarization yield was quantified by comparing the hyperpolarized signal to a thermally polarized reference (≈7 mL acetone, at natural abundance, ≈0.1 mol ^{13}C). See supplementary information for more details.

Experiments Using an NMR Spectrometer

NMR System and Experimental Setup: Experiments were performed on an NMR spectrometer (Avance III HD 300 MHz, Bruker, Germany) using a dual-channel ^{1}H/broad band probe head (5 mm PA BBO 300S1 BBF-H-D-05-Z) at a magnetic field of 7 T. The setup follows an idea similar to a setup described before[48] (denoted by **setup 3**).

***p*H$_2$ Enrichment**: The pH_2 fraction was enriched to ~90% using a commercial pH_2 converter (BPHG90, Bruker, Germany) at 36 K. The generator was used with a pH_2 pressure in the outlet path of ~9.2 bar.

Sample Preparation: SUC was formed by catalytic hydrogenation (same catalyst as already described) in the magnet bore of the NMR spectrometer at 66 °C in-bore temperature. In contrast to experiments on the preclinical MRI system, a different buffer solution was used: 0.04 g anhydrous sodium acetate (CAS: 127-09-3, Sigma Aldrich) was dissolved in 8.4 mL D_2O and about 1.55 mL glacial acetic acid (CAS: 64-19-7, Sigma Aldrich) was added to adjust the pH to 2.9 (HI 9124, Hanna instruments, USA). Subsequently, the solution was diluted to 9 mL with D_2O. The pH value remained at 2.9.

Experimental Workflow: Nine parts of buffer solution and one part (30 µL) of catalyst-substrate solution were filled into an NMR tube (total ≈300 µL solution, pH 2.9) and placed in the bore heated to 66 °C.

After manual shimming and matching, pH_2 was injected for t_{pH2} = 10 s via tubing connection to the pH_2 converter. Subsequently, the bypass was opened for t_{bypass} = 5 s, resulting in a total hydrogenation time of t_{hydr} = 15 s. PASADENA experiments with 45° ^{1}H excitation were performed (experiment E7).

2. Results

2.1. Hyperpolarization of Succinate

The values of the free evolution intervals that give optimal polarization for PH-INEPT+ and Goldman's sequence were simulated (Figure 1; Table 2) and are in agreement with previously reported simulations.[43] Using PH-INEPT+ and setup 1, SUC was polarized to P = (1.20 ± 0.15)% in a total number of three experiments with identical parameters (E1). Note, however, that 1-^{13}C,2,3,3-$^{2}H_3$-hydroxyethyl-propionate (HEP), an ABX-spin system, was polarized to ≈21% by SAMBADENA in a previous report using the same setup 1 and PH-INEPT+.[27]

When T-GM and decoupling ($t_{MLEV,90°}$ = 700 µs; Figure 4) were used for SUC in setup 2, the polarization drastically increased to P = (10.8 ± 0.6) %. Note that decoupling pulses were only applied during t_{bypass}, i.e. after bubbling with pH_2. The polarization was strongly dependent on the amplitude of the decoupling B_1 field (Figure 5): For short and long $t_{MLEV,90°}$, the polarization dropped significantly, likely because the transmit coil failed at high pulse power (short $t_{MLEV,90°}$) and because the excitation band width was too narrow when excitation pulses were long. Moreover, the polarization significantly decreased when off-resonant MLEV16 pulses were played out (Figure 6).

Table 2. Parameters and simulated polarization yield. The polarization level for SUC was determined for Goldman's sequence and PH-INEPT+ (Figure 1) depending on the state of the spin system after hydrogenation and before the SOT. Either a pure (with decoupling) or time-averaged singlet state (without heteronuclear decoupling during hydrogenation) was assumed. The total duration of SOT (t_{SOT}) is the sum of all the free evolution intervals. For the SOTs, on-resonant pulses, ideal flip angles were used and relaxation was neglected.

Sequence	Initial state	Intervalls / ms	t_{SOT} / ms	Polarization / %
PH-INEPT+	ρ_S	$t_{IN,1}$ = 70.84 ; $t_{IN,2}$ = 38.61	109.45	0
	$\overline{\rho_S}$			5.8
Goldman	ρ_S	$t_{G,1}$ = 27.87; $t_{G,2}$ = 36.84; $t_{G,3}$ = 50.78	115.49	99
	$\overline{\rho_S}$			56

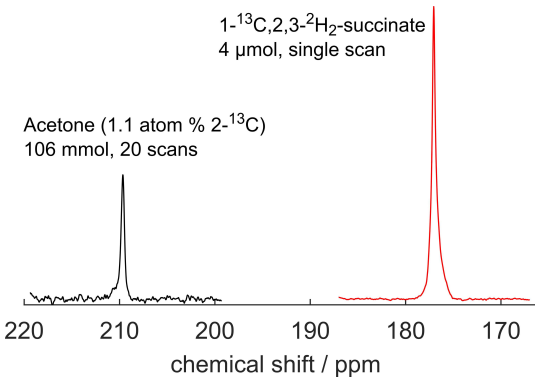

Figure 4. High SUC ^{13}C polarization > 10% was achieved using SAMBADENA and T-GM (Figure 1). Non-localized ^{13}C MR spectra of hyperpolarized SUC (176 ppm) and a thermally polarized acetone reference at natural abundance (210 ppm) were acquired at 7 T. For SAMBADENA, ^{1}H decoupling was applied during t_{bypass} and data acquisition ($t_{MLEV,90°}$ = 700 µs). With respect to the thermal reference, the maximal observed polarization was quantified to 11.9%, corresponding to a signal enhancement at 7 T of ≈20.000. Experimental details: setup 2, E4.

If decoupling was applied during the entire hydrogenation time (t_{pH2} and $t_{delay;}$ E3) prior to SOT, a much lower (≤1%) and strongly varying polarization was recorded for Goldman's sequence (L-GM; Figure 1) and setup 1. In this case, the polarization was independent of the amplitude of the MLEV16 decoupling field, i.e $t_{MLEV,90°}$. The polarization increased to (1.2 ± 0.8) % when decoupling was turned off entirely (six experiments, E2). Using setup 2, a polarization yield of (2.4 ± 0.2) % was obtained when decoupling was applied during the entire hydrogenation reaction (E6).

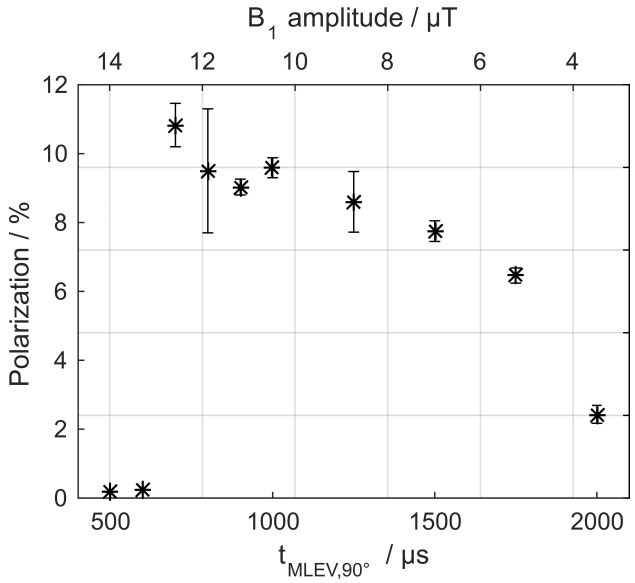

Figure 5. ^{13}C polarization of SUC by T-GM (Figure 1a) as a function of on-resonant decoupling pulses. A maximum polarization was observed for $t_{MLEV,90^\circ} = 700$ µs. For shorter pulses, much lower signal was observed. For each $t_{MLEV,90^\circ} > 600$ µs, three experiments were performed, for each $t_{MLEV,90^\circ} \leq 600$ µs, one. On the upper horizontal axis, the amplitude of the excitation field is given. Mean and standard deviation of the polarization are shown. Experimental details: setup 2, E4.

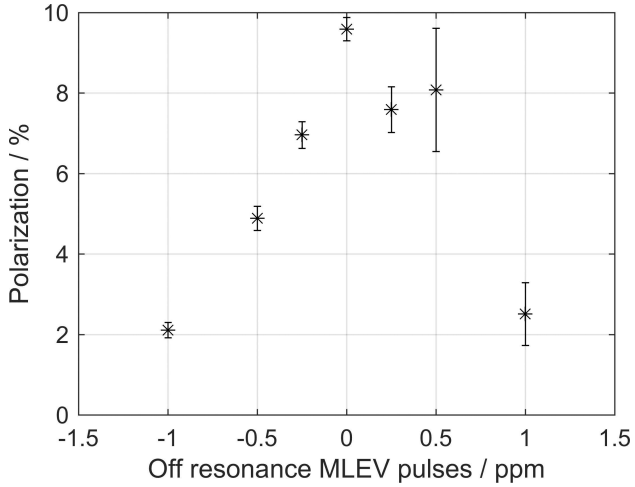

Figure 6. ^{13}C-polarization of SUC by T-GM (Figure 1a) as a function of the relative frequency offset of the decoupling pulses. Polarization decreased significantly when the frequency of the MLEV16 pulses was changed with respect to the center frequency of 2.7 ppm. For ±1 ppm off-resonance, polarization dropped from 9.5% to ~2%. Note that the ^{1}H and ^{13}C pulses of the SOT sequence (T-GM) were always on resonant. Each data point shows the mean value and standard deviation of the polarization of three experiments. Note that the band width of 180° pulse is 640 Hz (2.1 ppm). Experimental details: setup 2, E4.

2.2. The Hydrogenation Reaction and the Effect of Decoupling

Simulations predict close to unity polarization (99%) for Goldman's sequence (Table 2). Experimentally, however, mean polarization levels of ≈11% were observed (E4). To investigate the

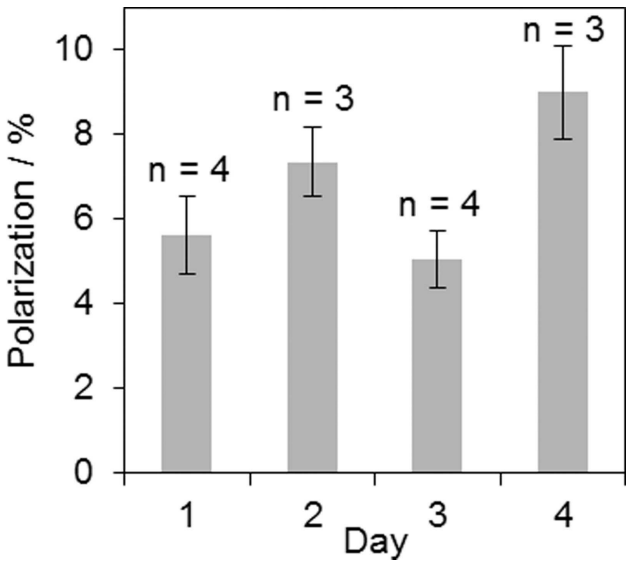

Figure 7. Reproducibility of ^{13}C polarization of SUC by L-GM (Figure 1). A mean polarization of (6.5 ± 1.7) % was obtained in 14 experiments on four days, detected one second after the SOT by a 90° acquisition. Decoupling pulse duration was set to $t_{MLEV,90^\circ} = 1$ ms and setup 2 was used. Error bars correspond to the standard deviation of n measurements of the respective day. Experimental details: E5.

reason for the reduced polarization, the density matrix after hydrogenation with pH_2 was analyzed for three settings: a) a single molecule without heteronuclear decoupling, b) ensemble of 5000 molecules without decoupling, and c) ensemble of 5000 molecules with decoupling (Figure 8).

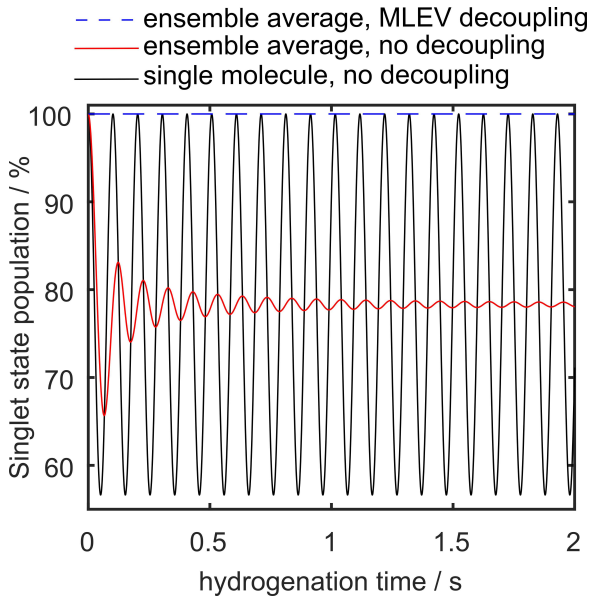

Figure 8. Simulated evolution of the singlet state population in SUC after addition of pH_2. For a single molecule, oscillations due to scalar interaction were observed (black line). These oscillations were damped to a constant value after ≈1.5 seconds if an ensemble of spins was considered that was hydrogenated at different points in time (red line). When heteronuclear decoupling pulses were applied to the ensemble, full singlet order was retained (blue dashed line). S-T_0 mixing was not considered here.

With HC-coupling intact, the population of the singlet state of the density matrix (Eq. 4) of a single molecule showed strong oscillations (Figure 8, black line). When an ensemble of spins was considered (Eq. 5, 6), these oscillations were damped to a quasi-constant singlet population of 78.4% after 1.5 s (Figure 8, red). The amplitude of the oscillations and the final value of singlet state population for infinite hydrogenation time depend on the J-coupling network of the spin system. Starting from this density matrix, a ^{13}C polarization of 56% and 5.8% was predicted for Goldman's sequence and PH-INEPT+, respectively (Table 1). When decoupling pulses (Eq. 5) were added, the full singlet order was preserved (Figure 8, blue dashed line). Here, a polarization yield of 99% was predicted for Goldman's sequence (Table 2). No polarization was found for PH-INEPT+.

These results indicate that decoupling and thus preservation of full singlet order has a strong impact on the polarization (e.g. drop of polarization from $P = 99\%$ to 56%). However, this polarization loss does not entirely explain the experimentally observed values ($P \approx 11\%$), where decoupling was applied for the last 3 of 5 s of the hydrogenation, implying a theoretical polarization of $\frac{2 \cdot 56 + 3 \cdot 99}{5}\% = 82\%$ (weighted sum).

2.3. The Effect of S-T_0 Mixing on the Polarization Yield

To elucidate the spin state after hydrogenation further, ^1H-PASADENA experiments were performed on an NMR spectrometer and compared to simulations. A 45° ^1H-acquisition ($t_{hydr} =$ 15 s) of SUC in D_2O revealed a significantly different line shape than was expected for pure time-averaged singlet state in an AA'X spin system (Figure 9, green and black line; Eq. 5, 6). When S-T_0 mixing was included in the simulations (Eq. 7), the basic features of the experiments were reproduced for $\lambda \cong 0.1$ (Figure 9, red line). The (unknown) S-T_0 mixing factor, λ, was estimated by manually adjusting λ to match the relative intensities of the simulated to the experimental spectra (Figure 9).

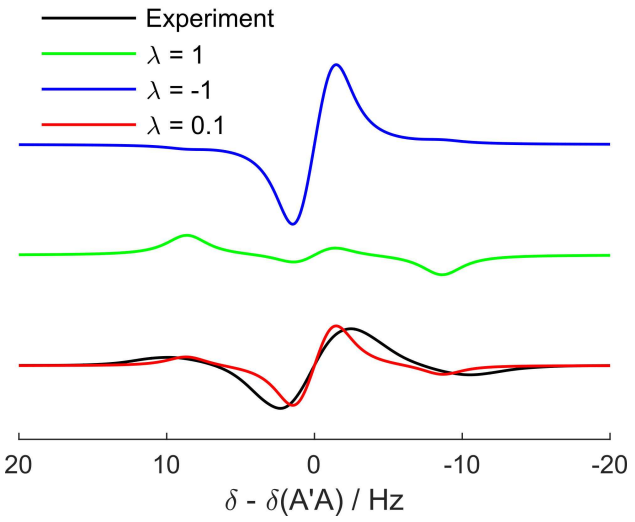

Figure 9. Experimental and theoretical ^1H PASADENA spectra (E7). The features of the experimental spectrum (black line) were reproduced by simulations (red line) when the S-T_0 mixing factor λ was set to ~0.1. Hence, the experimental spectrum is a superposition of time-averaged singlet (green line, $\lambda = 1$) and triplet state (blue line, $\lambda = -1$).

When S-T_0 mixing was taken into account, the simulated ^{13}C polarization using Goldman's sequence was drastically reduced: for a mixing factor of 0.1 (Figure 9), simulations revealed a polarization of 9.9% with decoupling (Eq. 8). When the spins were considered to evolve freely for two seconds and for another three seconds under ^1H decoupling (similar to experiments in Figure 4, 5 and 6), the polarization yield further decreased to 8.2%. This simulated polarization corresponds well to the observed values (Table 3).

Table 3. Experimental and theoretical polarization yield considering S-T_0 mixing. The polarization was simulated assuming different initial spin orders at the onset of SOT (singlet-triplet mixing without or with decoupling; Eq. 7 or 8). The mixing factor, λ, was set to 0.1. When a weighted sum (reflecting the fact that the spins evolve freely for two seconds and decoupling is applied only for three seconds), the polarization decreased to 8.2%.

	Simulated polarization / %		Experimental polarization / %	
Sequence	$\overline{\rho_{S/T_0}}$ w/o decoupling	ρ_{S/T_0}^{DEC} with decoupling	w/o decoupling	with decoupling
PH-INEPT+	8		1.2	
Goldman	5.6	9.9	1.2	10.8

3. Discussion

To achieve high polarization, it was key using Goldman's sequence for strongly coupled hydrogens and to start the decoupling only after the bubbling of the pH_2 injection. The reason for the variations in the inter-day polarization are unknown, but may be attributed to varying pH_2 enrichment, degassing of the solvent and flip angle variations, e.g. because of different matching of the coil. PH-INEPT+ did not yield high polarization because it was designed to transfer double spin order in weakly coupled ABX systems that is not the case for SUC.

3.1. Sources of Polarization Loss

3.1.1. Initial Spin State and S-T_0 Mixing

^1H-PASADENA experiments strongly indicate a substantial loss of singlet order due to S-T_0 mixing. Thus, the actual state of the density matrix after hydrogenation appears to be significantly different than the ideal one.

A mixing factor of $\lambda = 0.1$ implies that 45% of singlet order is lost during hydrogenation, resulting in a 10-fold reduction of polarization yield in the case of Goldman's sequence. S-T_0 mixing may be reduced by using another catalyst for hydrogenation since the chemical shift difference and contact time may differ. It should be noted that important steps have been

made in the last years in developing new biphasic or heterogeneous PHIP catalysts.[49–53]

To predict the mixing factor λ by calculations, the values of the chemical shifts and contact time in the reaction intermediate are required. However, the lifetime of the catalyst-SUC-pH$_2$-intermediate is short on the NMR time scale and the relevant values cannot be determined experimentally. Therefore, the phenomenological approach (comparison of experimental with theoretical PASADENA spectra) is the only available option to determine the value of λ.

3.1.2. Injection of pH_2 and Decoupling Efficiency

The loss of polarization and poor reproducibility when MLEV16 is applied during bubbling (t_{pH2}) is likely attributed to strong field inhomogeneities, caused by the bubbles, which in turn cause arbitrary excitations and thus depletion of spin order (see supplementary information for details). This hypothesis is supported by the finding that the polarization yield was much reduced when an off-resonance was added to the MLEV16 pulses on purpose (Figure 6).

Broader radio frequency pulses, i.e. shorter pulses along with a more efficient resonator may further increase the polarization. Moreover, MLEV16 irradiation on the carbon channel may also increase the polarization yield. First, ^{13}C decoupling during bubbling is likely less destructive since susceptibility effects are reduced by a factor of four (gyromagnetic ratio: $\gamma_H/\gamma_C \approx 4$). Second, protons are continuously added to the molecules and are thus not exposed to full ^{1}H-MLEV16 cycles. By applying ^{13}C-MLEV16 instead, ^{13}C-spins always experience complete MLEV16 cycles. However, ^{1}H/^{2}H couplings would remain when using ^{13}C-MLEV16. This and other heteronuclear decoupling schemes like WALTZ16[54] are currently under investigation.

It should be noted that in setup 2, hydrogenation carries on for two seconds without decoupling during t_{pH2} and time evolution of the spin states occurs during this time.

3.2. Comparision with SOT at low Field

A polarization of (5.4 ± 1.3) % of 1-^{13}C, 2,3-^{1}H$_2$-succinate in H_2O was measured before and estimated to a nascent polarization of (12.9 ± 3.1) % after hyperpolarization at low field.[17] Similar results were found by *Chekmenev et al.*: (17.6 ± 1.4) % of ^{13}C spin polarization at the time point of production was reported.[44]

These values are comparable to those reported in this paper. In these experiments at low field,[17,44] decoupling was applied during the entire hydrogenation reaction prior to the application of Goldman's sequence. The hydrogenation reaction was initialized by spraying FUM in aqueous catalyst solution into a pH_2 atmosphere. The much lower field strength (mT instead of 7 T) decreases off-resonance effects caused by susceptibility differences in the sample volume. Moreover, S-T$_0$ mixing may vary as well.

4. Conclusion

High and reproducible ^{13}C-hyperpolarization of the biomolecule SUC ≈11% was achieved by SAMBADENA within an MRI system. Important insights into the spin order transfer physics at high magnetic field were gained. Pitfalls of the experimental implementation were found, as decoupling during bubbling strongly deteriorates the polarization. Singlet-Triplet mixing was identified as a likely dominant source of spin order loss. Overall, these results are an important step towards the cost efficient and fast preclinical application of a hyperpolarized biomolecule *in vivo*. SAMBADENA[27] hyperpolarization is particularly interesting in the light of the recently reported *in vivo* application[28] and pH$_2$-hyperpolarization of metabolic agents like pyruvate and acetate by PHIP-SAH.[25,40,55]

Acknowledgements

Support by the Emmy Noether Program of the DFG (HO 4604/2-1, 4604/2-2), the German Consortium for Translational Cancer Research (DKTK), the Cluster of Excellence "Inflammation at Interfaces" (EXC306), "Precision Medicine in Inflammation" (PMI 1267), a grant of the RFBR and DFG (HO-4604/3-1, 19-53-12013), the European Union's Horizon 2020 research and innovation programme under the Marie Sklodowska-Curie grant agreement No 642773 and the Heinrich-Böll-Stiftung (ABS, P131623) is gratefully acknowledged. We thank the mechanical workshop of the University Medical Center Freiburg, in particular Waldemar Schimpf for excellent work. Furthermore, we wish to thank Kiel University and the Medical Faculty for supporting the Molecular Imaging North Competence Center (MOIN CC) as core facility for imaging in vivo. MOIN CC was founded by a grant of the European Regional Development Fund (ERDF) and the Zukunftsprogramm Wirtschaft of Schleswig-Holstein (Project no. 122-09-053). We thank Sergey Korchak and Salvatore Mamone for help and advice on the NMR spectrometer.

Conflict of Interest

The authors declare no conflict of interest.

Keywords: nuclear magnetic resonance · hyperpolarization · parahydrogen · biomolecules · succinate derivatives

[1] U. Ludwig, A.-K. Eisenbeiss, C. Scheifele, K. Nelson, M. Bock, J. Hennig, D. v. Elverfeldt, O. Herdt, T. Flügge, J.-B. Hövener, *Sci. Rep.* **2016**, *6*, 23301.
[2] M. Markl, A. Frydrychowicz, S. Kozerke, M. Hope, O. Wieben, *J. Magn. Reson.* **2012**, *36*, 1015–1036.
[3] A. Toutios, S. S. Narayanan, *APSIPA Trans Signal Inf Process* **2016**, *5*.
[4] S. Niesporek, C. Niesporek, R. Umathum, J. M. Lommen, N. G. R. Behl, D. Paech, P. Bachert, M. E. Ladd, A. Nagel, *Magn. Reson. Med.* **2018**, *79*, 2923–2934.
[5] T. Platt, R. Umathum, T. M. Fiedler, A. M. Nagel, A. K. Bitz, F. Maier, P. Bachert, M. E. Ladd, M. O. Wielpütz, H.-U. Kauczor, N. G. R. Behl, *Magn. Reson. Med.* **2018**, *80*, 1005–1019.

[6] A. M. Nagel, F. Lehmann-Horn, M.-A. Weber, K. Jurkat-Rott, M. B. Wolf, A. Radbruch, R. Umathum, W. Semmler, *Radiology* **2014**, *271*, 585–595.
[7] R. Borowiak, J. Groebner, M. Haas, J. Hennig, M. Bock, *Magn. Reson. Mater. Phys. Biol. Med.* **2014**, *27*, 95–99.
[8] J. H. Ardenkjaer-Larsen, B. Fridlund, A. Gram, G. Hansson, L. Hansson, M. H. Lerche, R. Servin, M. Thaning, K. Golman, *Proc. Natl. Acad. Sci. U. S. A.* **2003**, *100*, 10158–10163.
[9] C. H. Cunningham, J. Y. C. Lau, A. P. Chen, B. J. Geraghty, W. J. Perks, I. Roifman, G. A. Wright, K. A. Connelly, *Circ. Res.* **2016**, *119*, 117–1182.
[10] S. J. Nelson, J. Kurhanewicz, D. B. Vigneron, P. E. Z. Larson, A. L. Harzstark, M. Ferrone, M. v. Criekinge, J. W. Chang, R. Bok, I. Park, G. Reed, L. Carvajal, E. J. Small, P. Munster, V. K. Weinberg, J. H. Ardenkjaer-Larsen, A. P. Chen, R. E. Hurd, Liv-Ingrid Odegardstuen, F. J. Robb, J. Tropp, J. A. Murray, *Sci. Transl. Med.* **2014**, *5* .
[11] R. Aggarwal, D. B. Vigneron, J. Kurhanewicz, *Eur. Urol.* **2017**, *72*, 1028–1029.
[12] P. Wespi, J. Steinhauser, G. Kwiatkowski, S. S. Kozerke, *Magn. Reson. Med.* **2018**, *80*, 1882–1890.
[13] T. C. Eisenschmid, R. U. Kirss, P. P. Deutsch, S. I. Hommeltoft, R. Eisenberg, J. Bargon, R. G. Lawler, A. L. Balch, *J. Am. Chem. Soc.* **1989**, *109*, 8089–8091.
[14] C. R. Bowers, D. P. Weitekamp, *Phys. Rev. Lett.* **1986**, *57*, *2645–2648*.
[15] C. R. Bowers, D. P. Weitekamp, *J. Am. Chem. Soc.* **1987**,109,5541-5542.
[16] H. Jóhannesson, O. Axelsson, M. Karlsson, *C. R. Phys.* **2004**, *5*, 315–324.
[17] J.-B. Hövener, E. Y. Chekmenev, K. C. Harris, W. H. Perman, T. T. Tran, B. D. Ross, P. Bhattacharya , *MAGMA.* **2009**, *22*, 123–134.
[18] J.-B. Hövener, E. Y. Chekmenev, K. C. Harris, W. H. Perman, L. W. Robertson, B. D. Ross, P. Bhattacharya, *MAGMA.* **2009**, 22, 111–121.
[19] S. Kadlecek, V. Vahdat, T. Nakayama, D. Ng, K. Emami, R. Rizi, *NMR Biomed.* **2011**, 24, 933–942.
[20] K. W. Waddell, A. M. Coffey, E. Y. Chekmenev, *J. Am. Chem. Soc.* **2011** *133*, 97–101.
[21] J. Agraz, A. Grunfeld, K. Cunningham, D. Li, S. Wagner, *J. Magn. Reson.* **2013**, 235, 77–84.
[22] J. Agraz, A. Grunfeld, D. Li, K. Cunningham, C. Willey, R. Pozos, S. Wagner, *Rev. Sci. Instrum.* **2014**, *85*, 044705.
[23] A. M. Coffey, R. Shchepin, M. L. Truong, K. Wilkens, W. Pham, E. Y. Chekmenev, *Anal. Chem.* **2016**, *88*, 8279–8288.
[24] M. Goldman, H. Jóhannesson, O. Axelsson, M. Karlsson, *C. R. Chim.* **2006**, *9*, 357–363.
[25] F. Reineri, T. Boi, S. Aime, *Nat. Commun.* **2015**, *6*, 5858.
[26] R. Borowiak, N. Schwaderlapp, F. Huethe, T. Lickert, E. Fischer, S. Bär, J. Hennig, D. v. Elverfeldt, J.-B. Hövener, *MAGMA* **2013**, 491–499.
[27] A. B. Schmidt, S. Berner, W. Schimpf, C. Müller, T. Lickert, N. Schwaderlapp, S. Knecht, J. G. Skinner, A. Dost, P. Rovedo, J. Hennig, D. v. Elverfeldt, J.-B. Hövener, *Nat. Commun.* **2017**, *8*, 14535.
[28] A. B. Schmidt, S. Berner, M. Braig, M. Zimmermann, J. Hennig, D. v. Elverfeldt, J.-B. Hövener, *PLoS One*, **2018**, *13*.
[29] P. Bhattacharya, E. Y. Chekmenev, W. H. Perman, K. C. Harris, A. P. Lin, V. A. Norton, C. T. Tan, B. D. Ross, D. P. Weitekamp, *J. Magn. Reson.* **2007**, *186*, 150–155.
[30] N. M. Zacharias, C. R. McCullough, S. Wagner, N. Sailasuta, H. R. Chan, Y. Lee, J. Hu, W. H. Perman, C. Henneberg, B. D. Ross, P. Bhattacharya, *J. Mol. Imaging Dyn.* **2016**, *6*, 1–9.
[31] K. L. Billingsley, S. Josan, J. M. Park, S. S. Tee, E. Spielman-Sun, R. Hurd, D. Mayer, D. Spielman, *NMR Biomed.* **2014**, *27*, 356–362.
[32] E. Cavallari, C. Carrera, T. Boi, S. Aime, F. Reineri, *J. Phys. Chem. B* **2015**, *119*, 10035–10041.
[33] M. Haake, J. Natterer, J. Bargon, *J. Am. Chem. Soc.* **1996**, 118, 8688–8691.
[34] M. Goldman, H. Jóhannesson, *C. R. Phys.* **2005**, *6*, 575–581.
[35] S. Kadlecek, K. Emami, M. Ishii, R. Rizi, *J. Magn. Reson.* **2010**, *205*, 9–13.
[36] C. Cai, A. M. Coffey, R. V. Shchepin, E. Y. Chekmenev, K. W. Waddell, *J. Phys. Chem. B.* **2013**, *117*, 1219–1224.
[37] V. A Norton, PhD thesis, California Institute of Technology, **2010**.
[38] G. Stevanato, J. Eills, C. Bengs, G. Pileio, *J. Magn. Reson.* **2017**, *277*, 169–178.
[39] G. Stevanato, *J. Magn. Reson.* **2017**, *274*, 148–162.
[40] S. Korchak, S. Yang, S. Mamone, S. Glöggler, *ChemistryOpen,* **2018**, *7*, 344–348.
[41] J. Eills, G. Stevanato, C. Bengs, S. Glöggler, S. J. Elliott, J. Alonso-Valdesueiro, G. Pileio, M. H. Levitt, *J. Magn. Reson.* **2017**, *274*, 163–172.
[42] M. H. Levitt, R. Freeman, R. T. Frenkiel, *J. Magn. Reson.* **1982**, *47*, 328–330.
[43] S. Bär, T. Lange, D. Leibfritz, J. Hennig, D. v. Elverfeldt, J.-B. Hövener, *J. Magn. Reson.* **2012**, *225*, 25–35.
[44] E. Y. Chekmenev, J.-B. Hövener, V. A. Norton, K. Harris, L. S. Batchelder, P. Bhattacharya, B. D. Ross, D. P. Weitekamp, *J. Am. Chem. Soc.* **2008**, *130*, 4212–4213.
[45] J. Natterer, O. Schedletzky, J. Barkemeyer, J. Bargon, S. J. Glaser, *J. Magn. Reson.* **1998**, *133*, 92–97.
[46] O. W. Sørensen, G. W. Eich, M. H. Levitt, G. Bodenhausen, R. R. Ernst, *Prog. Nucl. Magn. Reson. Spectrosc.* **1984**, *16*, 163–192.
[47] J.-B. Hövener, S. Bär, J. Leupold, K. Jenne, D. Leibfritz, J. Hennig, S. B. Duckett, D. v. Elverfeldt, *NMR Biomed.* **2013**, *26*, 124–131.
[48] A. S. Kiryutin, G. Sauer, S. Hadjiali, A. V. Yurkovskaya, H. Breitzke, G. Buntkowsky, *J. Magn. Reson.* **2017**, *285*, 26–36.
[49] I. V. Koptyug, K. V. Kovtunov, S. R. Burt, M. S. Anwar, C. Hilty, S. Han, A. Pines, R. Z. Sagdeev, *J. Am. Chem. Soc.* **2007**, 129, 5580–5586.
[50] K. V. Kovtunov, I. E. Beck, V. I. Bukhtiyarov, I. V. Koptyug, *Angew. Chem. Int. Ed.* **2008**, *47*, 1492–1495; *Angew. Chem.* **2008**, *120*, 1514–1517.
[51] K. V. Kovtunov, V. V. Zhivonitko, A. Corma, I. V. Koptyug, *J. Phys. Chem. Lett.* **2010**, *1*, 1705–1708.
[52] S. Glöggler, A. M. Grundfeld, Y. N. Ertas, J. McCormick, S. Wagner, P. P. Schlecker, L. S. Bouchard, *Angew. Chem. Int. Ed.* **2015**, ***54***, 2452–2456; *Angew. Chem.* **2015**, *127*, 2482–2486.
[53] F. Reineri, A. Viale, S. Ellena, T. Boi, V. Daniele, R. Gobetto, S. Aime, *Angew. Chem. Int. Ed.* **2011**, *50*, 7350–7353; *Angew. Chem.* **2011**, *123*, 7488–7491.
[54] A. J. Shaka, J. Keeler, T. Frenkiel, R. Freeman, *J. Magn. Reson.* **1983**, *52*, 335–338.
[55] E. Cavallari, C. Carrera, M. Sorge, G. Bonne, A. Muchir, S. Aime, F. Reineri, *Sci. Rep.* **2018**, *8*, 8366.

Manuscript received: April 17, 2019